PAPER

Self-assembled titanium phosphonate nanomaterial having a mesoscopic void space and its optoelectronic application†

Malay Pramanik, Astam K. Patra and Asim Bhaumik*

Here we report the synthesis of a new crystalline titanium phosphonate material (HTiP-7) having a self-assembled nanostructure and a mesoscopic void space without the aid of any surfactant or templating agent. The material has been synthesized hydrothermally through the reaction between benzene-1,3,5-triphosphonic acid (BTPA) and titanium(IV) isopropoxide at neutral pH at 453 K for 24 h. This hybrid phosphonate material has been thoroughly characterized by powder X-ray diffraction, N_2 sorption, HR TEM, FE SEM, TG-DTA, FT IR and UV-Vis diffuse reflectance spectroscopic studies. Two very well-known software packages, REFLEX and CELSIZ unit cell refinement programs, are employed to establish the triclinic crystal phase of this hybrid material (HTiP-7). Very tiny nanocrystals of HTiP-7 self-aggregated to form spherical nanoparticles of dimension *ca.* 25 nm together with a mesoscopic void space and good BET surface area (255 m^2 g^{-1}). The framework is thermally stable up to 650 K. The material showed excellent carrier mobility for photocurrent generation in the presence of a photosensitizer molecule (Rose Bengal). To the best of our knowledge this is the first report of a photon-to-electron energy transfer process over a dye doped titanium phosphonate nanomaterial.

Introduction

Organic–inorganic hybrid porous materials have attracted major research interest over the years and these developments could contribute significantly to the conversion of photon energy.[1] Metal organophosphonate materials are the most promising class of hybrid materials due to the fact that there are numerous possibilities to vary organic components in the precursor organophosphorous moiety/ligand leading to different modes of coordination and functionalization in the resulting solid matrix.[2] These metal phosphonates have found potential applications in optoelectronics,[3] catalysis,[4] heavy metal ion adsorption,[5] magnetism[6] and so on. Thus considerable attention has been paid to the design of new organophosphorous motifs bearing two or more binding sites. Among them biphosphonic acid and functionalized biphosphonic acids are worth mentioning here.[7] However, for biphosphonic acid or its derivatives the respective metal phosphonates are organically pillared and close proximity of the aryl pillars prevents nanoscale porosity in the framework.[8] So when the porosity is targeted, bulkier biphosphonic acid sources [3,3′,5,5′-

tetramethylbiphenylene-bis(phosphonate)] have to be used otherwise some 'diluting' agents such as alkyl phosphonic acid have to be added for random pillaring.[9] To date most of the reports made in this context are focused on the close-packed arrangements of the organic ligands in the metal–organic frameworks.[10] So to impede the close packing of the organic scaffolds, here we have used benzene-1,3,5-triphosphonic acid as the organophosphorus source molecule for the synthesis of self-assembled porous titanium phosphonate nanoparticles without using any additional building blocks or templates. We have designed the ligand (benzene-1,3,5-triphosphonic acid) as the organic scaffold molecule for the synthesis of organic–inorganic hybrid porous titanium phosphonate material to enhance the mechanical stability and flexibility of the material by increasing the number of coordination sites (and thus more cross-linking) over aromatic mono-phosphonic or diphosphonic acids.[10] Apart from this, the π–π stacking interaction among the aromatic rings, present in the hybrid material, may promote the formation of a self-assembled nanostructure with an inter-particle mesoscopic void space. Designing a mesoporous metal phosphonate without the aid of any surfactant or templating agent is very challenging.

On the other hand, considerable effort has been made for the modification of the TiO_2 surface with a variety of phosphonic acids to control the interfacial and bulk properties of the

Department of Materials Science, Indian Association for the Cultivation of Science, Jadavpur, Kolkata 700 032, India. E-mail: msab@iacs.res.in

resulting hybrid material such as hydrophobicity, porosity, optical and electronic properties.[11] However, the homogeneous incorporation of phosphonic acid groups into porous TiO_2 is really an exigent problem.[12] The inhomogeneity of the organic phosphonic acid groups in the porous TiO_2 materials can be easily minimized in the hybrid titanium phosphonate by using bridging organophosphorus precursor molecules, where two or more phosphate groups are attached to the same organic fragment. Thus, designing a new bridging organophosphorus precursor molecule and employing it as a precursor for the synthesis of hybrid titanium phosphonate materials having high surface areas is quite challenging.

In this context it is relevant to mention that porous titanium(IV) phosphonate materials are intensively used in catalysis,[13] selective ion adsorption,[14] proton conductivity,[15] photo-degradation[16] and so on. However, to date there is no report of porous titanium phosphonate based nanomaterials in the photo-induced enhancement of electrical conductivity. We have recently reported a porous titanium(IV) phosphate (MTiP-1) material using a non-ionic surfactant templating route. However, the material has relatively low surface area (193 m^2 g^{-1}), large mesopore size (7.03 nm) and is devoid of an organic scaffold in the framework.[17] So our aim was to develop a metal phosphonate material with large surface area bearing an aromatic organic bridging moiety and comparatively smaller pore aperture so that the guest photosensitizer molecule (organic dye) can hold strongly at the surface of the porous cavity. There are two ways to achieve this goal: firstly we can synthesize an ordered mesoporous titanium phosphonate material (having pore width compatible with the guest photosensitizer molecule) bearing a phosphonic acid as the precursor molecule through the surfactant templating pathway or secondly designing the porous organic–inorganic hybrid titanium phosphonate using aromatic phosphonic acid as a phosphorus precursor molecule and having nanoscale porosity generated through the self-assembly of tiny nanocrystals *via* the non-templating pathway for the inclusion of the photosensitizer molecule. Now the removal of templates or structure directing agents (SDA) keeping the order structure unperturbed to produce ordered mesoporous titanium phosphonate is really an exigent problem for the phosphate based mesostructured materials. Thus, we choose the latter strategy to develop a novel hybrid titanium phosphonate material having a mesoscopic void space for insertion of the photosensitizer molecule. Here we report a new self-assembled mesoporous titanium phosphonate nanomaterial by using 1,3,5-benzene triphosphonic acid as the organophosphorus source under hydrothermal conditions. We tactically entrapped a photosensitizer molecule[18] (organic dye, Rose Bengal) into the mesoscopic void space of the titanium phosphonate nanoparticles. The observed photocurrent for dye loaded porous titanium phosphonate (HTiP-7RB) is 13.5 times more than hybrid titanium phosphonate (HTiP-7) and 3500 times more than pure titanium phosphate synthesized in the absence of any aromatic organophosphorus precursor molecule. We compare this result of photoconductivity value with our previously reported organic sensitizer loaded porous TiO_2 materials; the increment of photocurrent for HTiP-7RB is *ca.* 32 times more than RB-meso-TiO_2 and *ca.* 19 times more than MT-1-RB.[19] There are a few reports on the synthesis of ordered mesoporous titanium phosphonate materials from various aliphatic phosphonic acid scaffolds.[15] But for designing materials with enhanced optoelectronic property, the presence of a chromophoric aromatic moiety in the porous framework is essential. However, to date no such report is available. Thus we design HTiP-7, which carries benzene-1,3,5-triphosphonic acid as the organophosphorus scaffold for the high photon-to-electron energy transfer process. To the best of our knowledge this is the first report of the self-assembled mesoporous titanium phosphonate using benzene-1,3,5-triphosphonic acid as the organophosphorous precursor and its excellent photoresponse upon dye loading.[20]

Experimental section

Materials

Commercially available 1,3,5-tribromobenzene (98%), triethylphosphite (98%), 1,3-diisopropylbenzene and titanium-isopropoxide (97%) were purchased from Sigma Aldrich, USA. Nickel(II) bromide (99%) was purchased from Avra Chemicals, India.

Synthesis of benzene-1,3,5-triphosphonic acid. 9.45 g of 1,3,5-tribromobenzene was dissolved in 75 ml 1,3-diisopropylbenzene by heating at 120 °C under a nitrogen atmosphere. The reaction mixture was cooled to 70 °C and anhydrous nickel(II) bromide (1.5 g) was added to the reaction mixture under vigorous stirring under an inert atmosphere. Then the reaction mixture was heated gradually to 180 °C and triethyl phosphite (22.5 ml) was added for 3 h. The heating was continued for the next 6 h at the same temperature under an inert atmosphere. Then the volatile component and 1,3-diisopropylbenzene were distilled off, and a dark viscous residue was obtained. The compound (hexaethyl-1,3,5-benzenetriphosphonate) was purified over a column of silica gel eluted with CHCl$_3$ [CHCl$_3$: MeOH = 10 : 1 (v/v)]. The colorless hexaethyl-1,3,5-benzenetriphosphonate was obtained by solvent evaporation and the yield was 5.85 g (40%). Then 4.5 g of the produced ester was hydrolyzed with 30 ml water in the presence of 30 ml concentrated HCl for 12 h. The hydrolyzed solution was evaporated to dryness and the residue was dissolved in 15 ml distilled water and decolorized by activated charcoal, then the filtrate was evaporated under reduced pressure to get a white solid, benzene-1,3,5-triphosphonic acid (BTPA)[21] having a yield of 2.7 g (92%). The compound was characterized by ^{1}H, ^{13}C, ^{31}P NMR and IR spectroscopy. ^{1}H NMR (500 MHz, D$_2$O) δ = 8.07 ((t, 3*J*PH) 15 Hz); ^{13}C NMR (500 MHz, D$_2$O) δ = 135.23; 136.07; ^{31}P NMR (500 MHz, D$_2$O) δ = 12.87. IR (KBr, cm^{-1}) ν_{max} 3387, 3088, 2925, 2319, 1142, 1001, 943, 691, 536, 470.

Synthesis of the self-assembled porous titanium(IV) phosphonate HTiP-7. In the typical synthesis of HTiP-7, 1.272 g (4.0 mmol) of benzene-1,3,5-triphosphonic acid was dissolved

Table 1 Change in BET surface area for the different titanium phosphonates synthesized at different pH and temperatures[a]

Sample name	Synthetic pH	Temperature (°C)	Surface area ($m^2 g^{-1}$)
HTiP-7	6–7	180	255
HTiP-7A	1–2	180	83
HTiP-7B	10	180	123
HTiP-7C	6–7	120	188
HTiP-7D	6–7	150	218

[a] Reaction time = 24 h.

in 10 ml double distilled water. Simultaneously, 6.818 g (24.0 mmol) of titanium-isopropoxide was dissolved in 10 ml dry iso-propanol in another dry beaker. The synthetic gel was prepared by very slow addition of the former acid solution to the alcoholic titanium-isopropoxide solution. The as syn-thesized gel was aged under stirring conditions overnight and then transferred into a Teflon-lined autoclave and kept at 453 K for 24 h. The autoclave was cooled to room temperature. The final suspension was centrifuged at 5000 RPM to collect the titanium(IV) phosphonate nanoparticles. Then the product was suspended in dry ethanol and again centrifuged to get the desired solid product (HTiP-7) and dried in a high vacuum pump for 5 h. The final product yield was 3.86 g. Keeping the molar ratio of Ti and BTPA and reaction time unaltered, we synthesized a few more titanium phosphonate samples (HTiP-7A, HTiP-7B, HTiP-7C and HTiP-7D) by varying the pH of the synthetic gel and hydrothermal temperature (Table 1).

Preparation of the sample for photoconductivity measurements

For the impregnation of Rose Bengal (RB) at the surface of the self-assembled mesoporous titanium phosphonate (HTiP-7) material, 0.25 g of RB was dissolved in 25 ml absolute ethanol and then 1.0 g of HTiP-7 was dispersed into this solution with continuous stirring. After 3 h, the resultant content was fil-tered and washed with absolute ethanol to remove the adhered RB bound to the external surface. Then the RB impregnated titanium phosphonate (HTiP-7RB) material was dried at room temperature overnight and used for photoconductivity measurements.
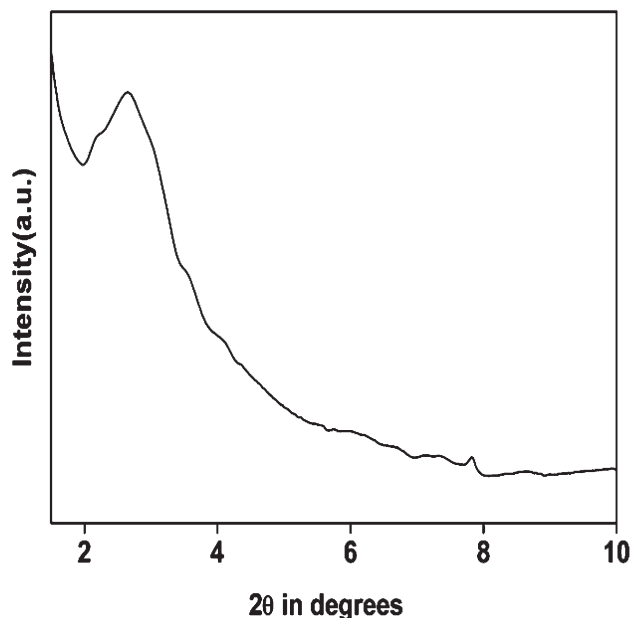
Instrumentation

Powder X-ray diffraction (PXRD) patterns were recorded on a Bruker D-8 Advance diffractometer operated at 40 kV and 40 mA and calibrated with a standard silicon sample, using Ni-filtered Cu Kα (λ = 0.15406 nm). Fourier transform infrared (FT IR) spectra of the materials were recorded using a Nicolet MAGNA-FT IR 750 Spectrometer Series II. Elemental analyses were carried out by using a Shimadzu AA-6300 atomic absorp-tion spectrophotometer (AAS) fitted with a double beam mono-chromator and a Perkin-Elmer 2400 Series-II CHN analyzer. A JEOL JEM 6700F field emission scanning electron microscope (SEM) was used for the determination of the morphology of powder samples. The pore structure was evaluated by using a

JEOL JEM 2010 high resolution transmission electron micro-scope (HR TEM) operated at an accelerating voltage of 200 kV. Nitrogen adsorption/desorption isotherms were obtained by using a Beckman Coulter SA 3100 surface area analyzer at 77 K. ^{1}H NMR and ^{13}C experiments were carried out on a Bruker DPX-300 NMR spectrometer. Thermogravimetric analy-sis (TGA) and differential thermal analysis (DTA) of the sample were carried out in a TGA instrument thermal analyzer TA-SDT Q-600 under a continuous flow of nitrogen with a heating/cooling rate of 10 °C min^{-1}. UV-visible diffuse reflectance spectra were recorded on a Shimadzu UV 2401PC with an inte-grating sphere attachment. $BaSO_4$ was used as the background standard. For the electrical measurements, firstly pellets of each of the samples of 1 cm diameter were made and two plati-num electrodes (of ca. 50 nm thickness) were attached on each pellet in the circular form of diameter 2 mm through a shadow mask at a separation of 4 mm. The DC current between the two electrodes was measured using a Keithley source meter (model 2420). The photocurrents were measured by illuminating with a 150 W xenon lamp light source (Newport Corp. USA; model no. 69907).

Results and discussion

Powder X-ray diffraction

The small angle powder X-ray diffraction pattern for HTiP-7 is shown in Fig. 1. One broad peak centered at 2θ = 2.64° could be attributed to the self-assembly of tiny titanium phospho-nate nanoparticles.[22] The interparticle distance corresponding to this broad diffraction is ca. 3.34 nm. The wide angle X-ray powder diffraction pattern for the HTiP-7 material is shown in Fig. 2. The very strong and sharp peaks in the wide angle

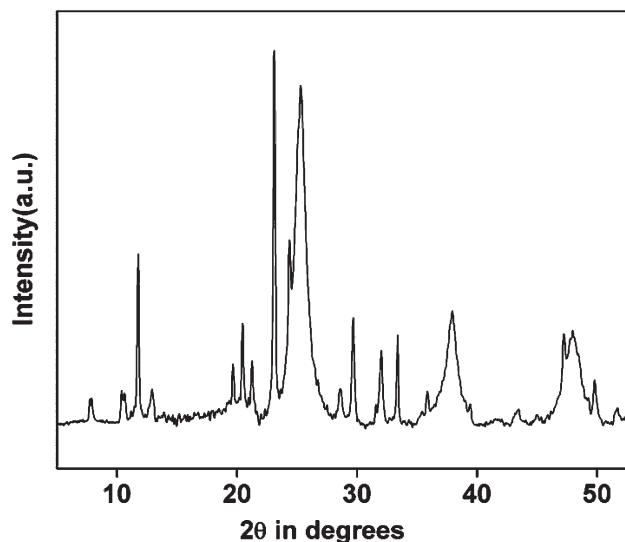**Fig. 1** Small angle powder XRD pattern of HTiP-7.

Fig. 2 Wide angle XRD pattern of HTiP-7.

Table 3 Indexing of triclinic crystal structure of HTiP-7

h	k	l	2θ (°)	d (Å)
0	1	1	7.732	11.424
1	0	0	7.883	11.214
1	1	0	10.390	8.513
0	1	2	10.633	8.319
1	1	1	11.746	7.533
1	−1	2	12.954	6.833
0	3	1	19.671	4.492
1	−3	−1	20.488	4.334
1	1	−5	21.286	4.174
1	−3	3	23.098	3.851
0	0	6	24.358	3.654
2	−3	−2	25.090	3.549
2	−3	2	25.356	3.512
0	1	−7	28.599	3.121
0	1	7	29.684	3.009
0	5	−1	31.584	2.832
0	5	−2	32.045	2.793
0	5	2	33.407	2.681
0	3	7	35.848	2.504
0	1	9	37.946	2.377
0	5	5	39.412	2.286
0	4	8	43.477	2.081
1	−7	4	47.223	1.924
0	7	−5	48.006	1.895
0	0	12	49.810	1.831
0	8	−1	51.679	1.768

diffraction pattern provide evidence of long range periodicity in the porous architecture. None of the peaks can be attributed to the typical crystalline TiO_2 peaks; hence the crystallinity of the material is due to the long range ordering of the pure titanium(IV) phosphonate framework.[23] When alcoholic titanium(IV) isopropoxide solution is added to the aqueous phosphonic acid solution, there is competition between the water molecule and the phosphonic acid groups to coordinate with the positively charged titanium. Strong coordinative interaction of a highly water soluble organophosphorus precursor (benzene-1,3,5-triphosphonic acid) with titanium(IV) could prohibit the formation of oxide material.[24]

Here we have used REFLEX software for indexing the crystal planes of highly crystalline porous titanium(IV) phosphonate nanoparticles and the extent of matching is verified with the CELSIZ unit cell refinement program. The wide angle X-ray diffraction pattern of HTiP-7 matches well with the triclinic crystal phase with unit cell parameters a = 11.328(0.018) Å, b = 14.184(0.005) Å, c = 22.227(0.010) Å, α = 94.486°(0.073), β = 97.279°(0.096), γ = 93.265°(0.065) (Table 2). The very high unit cell volume (V = 3523.863 Å^3) together with the quite small standard deviation (ESD = 5.59) is in good agreement with the triclinic crystal phase of HTiP-7. The reflections from different planes (hkl) of the polycrystalline material and the corresponding d spacings are given in Table 3.

Table 2 Unit cell parameters of HTiP-7

Parameters	Deviations
a = 11.328	0.018
b = 14.184	0.005
c = 22.227	0.010
α = 94.486	0.073
β = 97.279	0.096
γ = 93.265	0.065
V = 3523.863	ESD = 5.590

Spectroscopic study

The FT IR spectral bands between 4000 cm^{-1} to 400 cm^{-1} of HTiP-7 are shown in Fig. 3. The peak centered at 554 cm^{-1} is the characteristic peak for the Ti–O stretching vibration. No additional peak in the range <500 cm^{-1} confirms the absence of Ti–O–Ti bonding in the porous framework. The peak centered at 1040 cm^{-1} is due to the phosphonate (P–O–Ti) stretching vibration. The absence of a set of bands at 943 cm^{-1} and 1142 cm^{-1} confirms the absence of free P–OH and P=O in the porous matrix. Hence, it is expected that all P–O bonds are coordinated to titanium forming –P(O–Ti)$_3$ units[24] and the
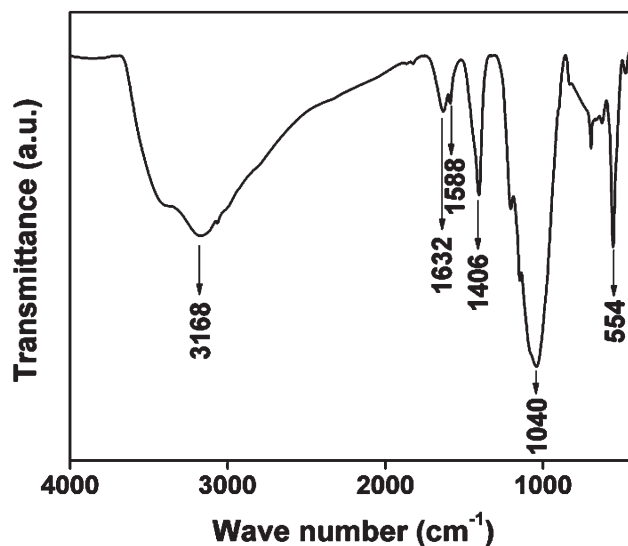

Fig. 3 FT IR spectrum of HTiP-7.

number of surface defect sites (P–OH) is very low. The characteristic peaks at 1406 and 1588 cm^{-1} confirm the presence of a benzene ring in the porous architecture.[21] A prominent peak at 1632 cm^{-1} could be attributed to the surface adsorbed water molecules.

Solid state MAS NMR studies

Solid state ^{13}C CP MAS and ^{31}P MAS NMR experiments generally provide information about the chemical environment around C and P nuclei in the hybrid metal phosphonate framework. In Fig. 4, the ^{13}C CP MAS NMR of HTiP-7 is shown. It exhibits two peaks at 130.7 ppm and 134.7 ppm with almost similar intensity, indicating the presence of two types of carbon with equal number (shown in the inset of Fig. 4). The ^{31}P MAS NMR of HTiP-7 is shown in Fig. 5. Only one peak at −1.11 ppm signifies that only the 111 type of bonding is present around P nuclei. This information further proves the presence of only –P–(O–Ti)$_3$– units around phosphorous nuclei.[25] These spectroscopic results further suggested the presence of an organic moiety in the porous titanium(ɪᴠ) phosphonate framework of HTiP-7.

Electron microscopic analysis

The characteristic HR TEM image of HTiP-7 is shown in Fig. 6A. It is seen from this image that the hybrid titanium phosphonate nanoparticles with uniform spherical morphology (particle size *ca.* 23–25 nm) are spread throughout the specimens. A closer view of the individual nanoparticle (Fig. 6B) revealed that white spots of dimension *ca.* 1.5 nm are distributed throughout the matrix of the nanoparticles (white spots marked with a white circle). The presence of these micropores in the framework of HTiP-7 could be attributed to the cross-linking of the organophosphorous ligand and titanium. The self-assembled nanostructure in the material is also seen in this high resolution image, where the individual tiny
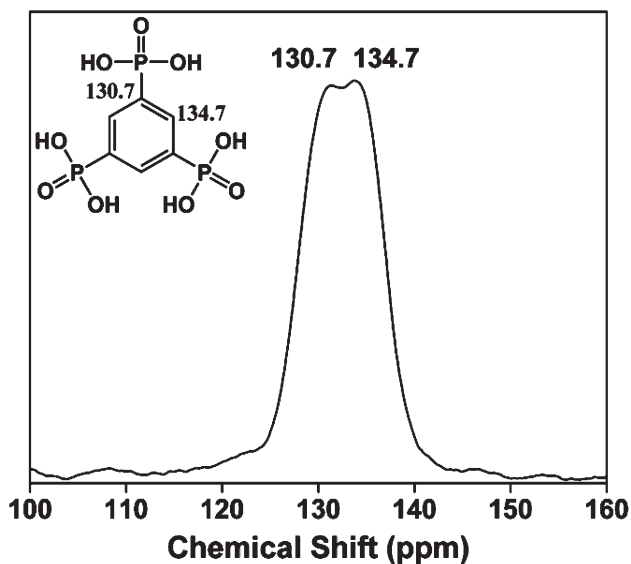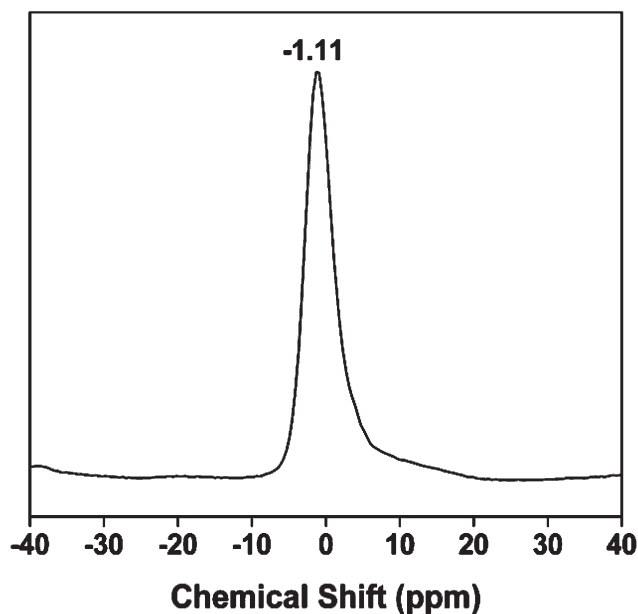

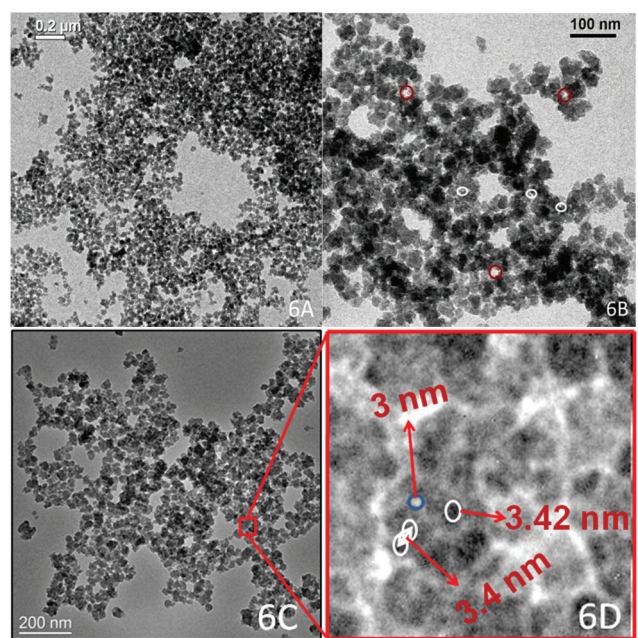**Fig. 5** ^{31}P MAS NMR spectrum of HTiP-7.

Fig. 6 HR TEM images of HTiP-7: low (A) and high (B) magnification; UHR-TEM images of HTiP-7: low (C) and high (D) magnification.

nanoparticles adhere to each other, maintaining a uniform distance between them. This self-assembled nanostructure is the origin of one broad small angle X-ray diffraction peak as shown above (Fig. 1). Further, the presence of medium and large size mesopores is quite clear from the high resolution electron microscopic image shown in Fig. 6B. Large interparticle mesopores of dimension *ca.* 4.8–5.0 nm are encircled with red circles in Fig. 6B. Further, the UHR-TEM analysis of HTiP-7 clearly proves the presence of medium and large size
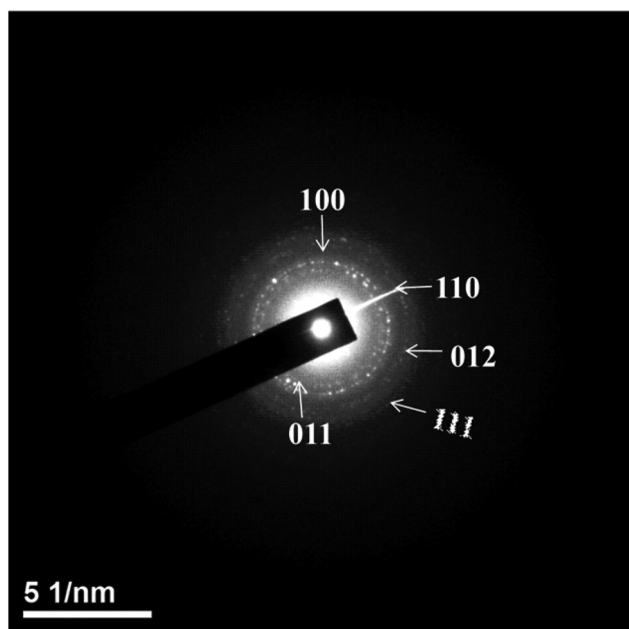

Fig. 4 ^{13}C MAS NMR spectrum of HTiP-7.

Fig. 7 SAED pattern of HTiP-7.

Fig. 8 FE SEM image of HTiP-7.

Fig. 9 TG (a) and DTA (a1) profiles of HTiP-7 and TG (b) and DTA (b1) profiles of HTiP-7RB.

mesopores throughout the specimen (Fig. 6C). A closer view of a small part of this specimen revealed that very tiny nanocrystals of dimension *ca.* 3.42 nm are self-aggregated to form medium size mesopores (*ca.* 3.0 nm) together with an interparticle distance of *ca.* 3.4 nm (Fig. 6D). Interparticle spacing as estimated through small angle powder XRD (Fig. 1) nicely resembles the electron microscopic data. The elemental mapping of the material with EDX analysis (Fig. S1†) clearly proves the presence of carbon, phosphorus, titanium and oxygen in the porous framework. The high crystallinity of the material has been supported by its well-resolved selected area electron diffraction (SAED) pattern shown in Fig. 7. The diffraction spots suggest the formation of a triclinic crystal phase of the hybrid material with indexed crystal planes. The FE-SEM image of the material is shown in Fig. 8. From this image it is clear that the hybrid titanium phosphonate material is composed of uniform spherical nanoparticles of dimension *ca.* 25 nm. Thus, the electron microscopic analysis reveals that the tiny microporous nanocrystals of *ca.* 3.5 nm size are self-assembled to form uniform aggregated spherical nanoparticles of *ca.* 25 nm dimension and mesoscopic void space in the hybrid material.[26]

Thermal analysis

The stability of the hybrid titanium(IV) phosphonate and the dye loading capacity of the material have been determined from the TG-DTA profile under air flow. The TG and DTA plots of the samples are shown in Fig. 9 (a and a1 plots correspond to the TG and DTA profiles of HTiP-7 and b and b1 correspond to those of HTiP-7RB). The TGA plot of HTiP-7 shows three distinct weight losses. The first 5.2% weight loss up to 373 K is attributable to the loss of intercalated and adsorbed water molecules in the sample. The second and third weight losses
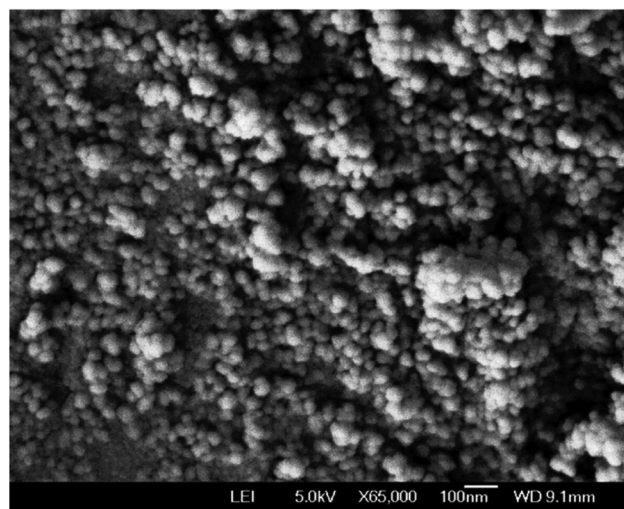
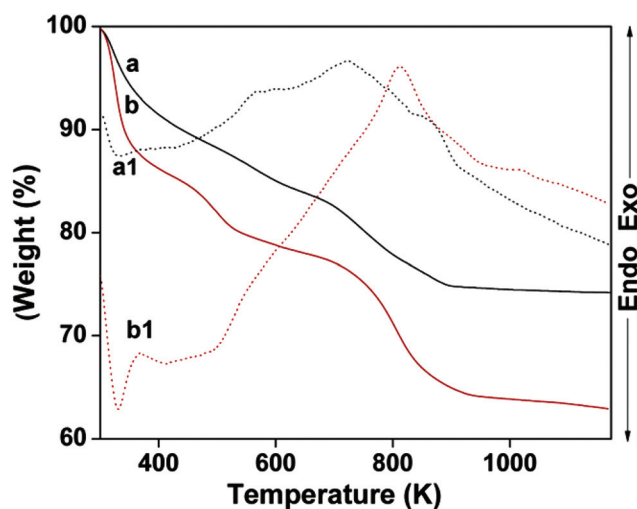correspond to the burning of organic fragments of the hybrid framework. The breaking of C–C, C–P and C–H bonds extended up to 900 K. The 20.4% weight loss of the material in this temperature interval is mainly due to the burning of the carbon fragment of the hybrid material. We have also carried out variable temperature powder XRD analysis of the titanium phosphonate material to understand the thermal stability (Fig. 10). As seen from the figure, the structure is very stable at 450 K. At 650 K a considerable decrease in the intensity of some of the major diffraction peaks is observed, whereas at 750 K many significant diffraction peaks disappear. At 900 K the crystallinity of the materials decreases hugely with some additional weak peaks around 2θ values 25.3°, 37.7°, 48.1° which could be attributed to the formation of anatase TiO_2 at higher temperature. The first 5.2% weight loss up to 373 K remained the same for HTiP-7Rb also. Now the second and third weight losses of HTiP-7RB correspond to the burning of
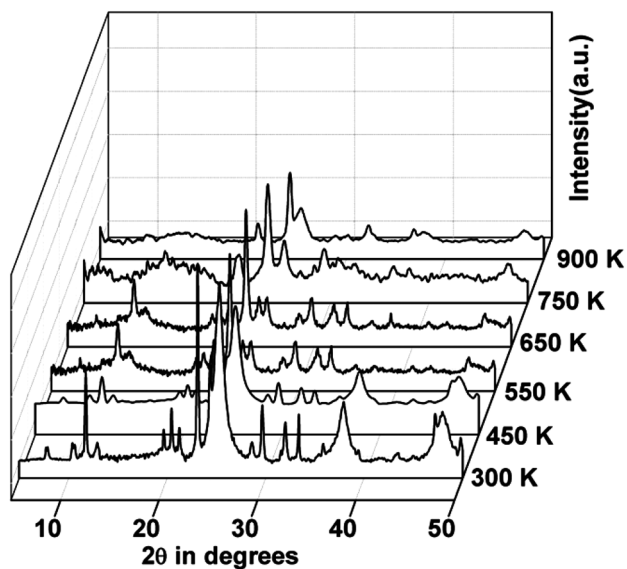
Fig. 10   Temperature variation XRD of HTiP-7.

Fig. 11 N_2 adsorption/desorption isotherm of HTiP-7. Adsorption points are marked by filled circles and those for desorption by open circles. NLDFT pore size distribution is shown in the inset.

organics in the hybrid framework and the adsorbed dye molecules. The breaking of bonds extended up to 900 K. Now the 30.5% weight loss in the temperature interval is due to the burning of carbon fragments of the hybrid material and adsorbed Rose Bengal molecules. Comparing the weight loss of HTiP-7 without dye loading, it can be concluded that HTiP-7 has 10.1% dye loading capacity, which is good to explore its potential in the photon-to-electron energy transfer process.

Molecular formula of HTiP-7

TG-DTA analysis of the sample HTiP-7 indicates the presence of 20.4 wt% organics in the material. On the other hand the CHN analysis data suggested the presence of 16.8 wt% C and 1.27 wt% H in this porous framework. Further, the atomic absorption spectroscopy (AAS) study revealed the presence of 25.9 wt% titanium in HTiP-7. From the FT IR and solid state ^{13}C and ^{31}P MAS NMR study, the presence of benzene-1,3,5-triphosphonic acid in the porous framework is confirmed. Taking all these elemental analysis results into consideration, the molar ratio of carbon : titanium in HTiP-7 is 2.59. Thus, the probable molecular formula of the porous architecture of HTiP-7 can be written as $Ti_9[C_6H_3(PO_3)_3]_{3.89} \cdot xH_2O$. Hence the formula of HTiP-7 can be expressed as $Ti_9(BTPA)_4 \cdot xH_2O$.

N_2 absorption/desorption

The porosity and surface area of the hybrid material are determined from the N_2 adsorption/desorption isotherm at 77 K. The adsorption/desorption isotherm of the material is shown in Fig. 11. The isotherm can be classified as a type IV isotherm[27] with an H3 hysteresis loop.[28] If we analyze the isotherm very closely, then we can see that at the pressure range (P/P_0) 0.1–0.2 the curve is all about flat, characteristic of a type I isotherm indicating the presence of relevant amounts of micropores in the material. After (P/P_0) 0.2, the multilayer
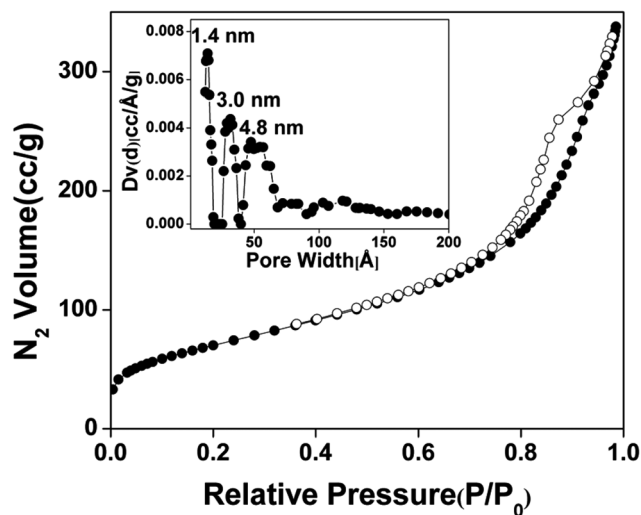
adsorption takes place and a strong capillary condensation is observed at the relative pressure of 0.60–0.97, suggesting the presence of appreciable amounts of mesopores in the material. The isotherm does not saturate in the higher relative pressure also, suggesting the presence of a small to large range of mesopores in the material. Due to the presence of applicable amounts of mesopores in HTiP-7, at the higher relative pressure $(P/P_0 > 0.7)$ the capillary evaporation and condensation do not take place at the same pressure, which leads to production of a hysteresis loop.[29] The Brunauer–Emmett–Teller (BET) surface area of the material is 255 m^2 g^{-1} with a total pore volume of 0.4635 cc g^{-1}. The pore size distribution of the material has been done from the non-local density functional theory (NLDFT)[30] and is shown in the inset of Fig. 11. The pore size distribution peak is centered at 1.4, 3.0, and 4.8 nm, suggesting that the material contains the pore in the supermicropore to large mesopore region. This result agrees very well with the HR TEM analysis described above. The molecular dimension calculated by using MOPAC-2012 software suggested that the size of the Rose Bengal molecule is 1.2 nm. So the photosensitizer molecule (RB) can fit inside the porous architecture composed of micro- and mesopores of HTiP-7. For the samples synthesized under strongly acidic conditions (pH ~ 1) some of the phosphonic acid source remains protonated, hence the cross-linking and formation of the three dimensional porous framework (HTiP-7A) is considerably disturbed. This is reflected in its low BET surface area (83 m^2 g^{-1}). On the other hand for the synthesis of titanium phosphonate under relatively strongly alkaline conditions, as the pH of the medium increases (pH ~ 10) a handsome amount of titanium could be converted to titanium oxide (TiO_2), which blocks the pores of the HTiP-7 framework. Hence, the BET surface area of the resulting sample HTiP-7B is also low (123 m^2 g^{-1}) compared to HTiP-7. The observed optimum temperature for the maximum number of cross-linking of Ti

and benzene-1,3,5-triphosphonic acid is 180 °C. At lower temperatures (120 and 150 °C), somehow the cross-linking between organo phosphonic acid and titanium is hampered, which is the probable reason behind the relatively lower surface area of the samples HTiP-7C (188 m^2 g^{-1}) and HTiP-7D (218 m^2 g^{-1}). Corresponding adsorption/desorption isotherms and pore size distributions are shown in ESI (Fig. S2 and S3†), which also suggested lack of mesopore contribution compared with HTiP-7 (Fig. 11).

UV-visible spectroscopy

The UV-visible reflectance spectra of the samples are shown in Fig. 12. The bulk titanium phosphate (synthesized by using H$_3$PO$_4$ as the P source under identical synthesis conditions) showed absorption maxima at 258 nm, while hybrid titanium phosphonate (HTiP-7) showed absorption maxima at 303 nm. The corresponding band gap energies are 3.42 and 2.82 eV, respectively. Basically HTiP-7 is the system where one free hydroxyl group (–OH) attached to phosphorous of bulk titanium phosphate has been replaced by a large conjugated organic system (benzene-1,3,5-triphosphonic acid). Due to the incorporation of a π-conjugated system into the bulk system the energy gap between HOMO and LUMO is decreased compared to bulk titanium phosphate, which has been reflected in the corresponding UV-Vis reflectance spectrum and the decrease in band gap energy.[31] Respective band gap energies for the materials are shown in Fig. 13. On the other hand, a complicated UV-Vis reflectance spectrum arises for dye encapsulated HTiP-7 material with the absorption maxima at 557, 520 and 312 nm. The respective band gap energy is 2.05 eV. The red shift of the UV-Vis spectrum of HTiP-7RB from 303 nm of HTiP-7 could be attributed to the interaction of the titanium phosphonate molecular orbital by Rose Bengal through RB → HTiP-7 charge transfer.[32]
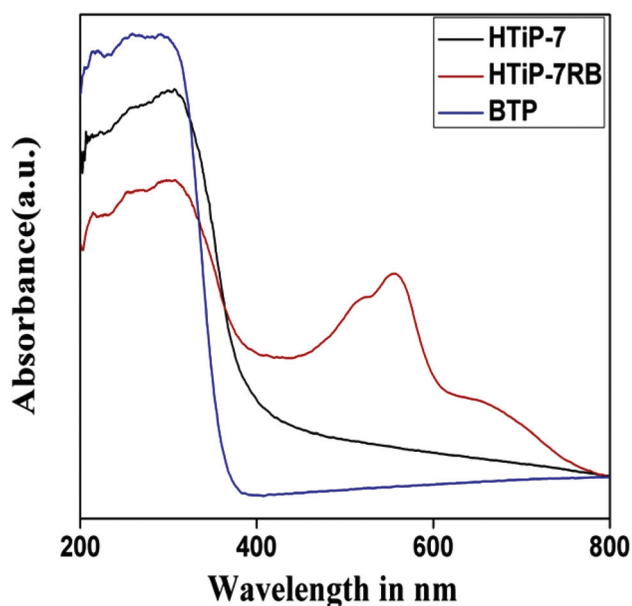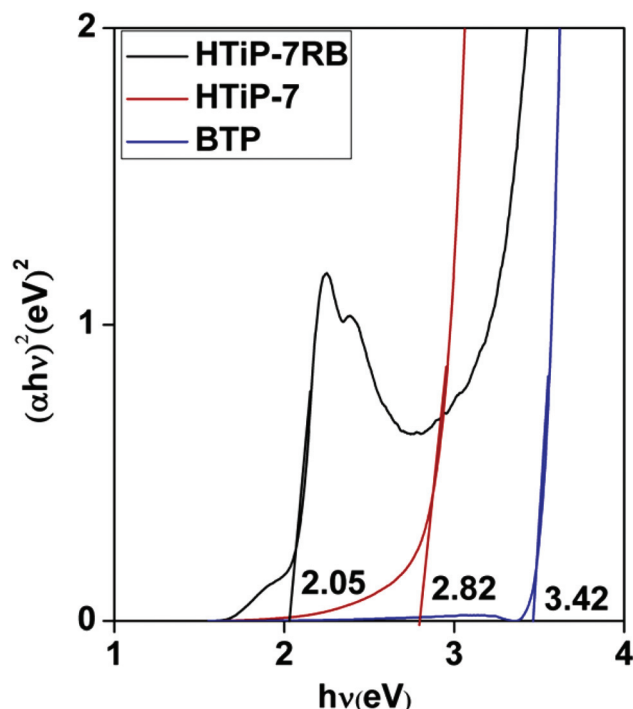

Fig. 13 Band gap energies of BTP, HTiP-7, HTiP-7RB.

Photoconductivity

Bulk titanium phosphate (BTP), HTiP-7 and dye-loaded hybrid titanium phosphonate HTiP-7RB were kept in the dark overnight before measuring the dark current.[33] Linearity in the I–V characteristic curve proves the ohmic behavior[34] of platinum contacts on the samples (Fig. 14). From Fig. 14 it is clear that HTiP-7RB conducts much more current than HTiP-7 and BTP in the dark. Now to measure the light driven photoconductivity of the materials, we excited the surface of the materials (BTP, HTiP-7 and HTiP-7RB) with white light. In Fig. 15 we have shown the growth/decay current for the materials at 10 V bias. As soon as the white light irradiates the surface of materials,
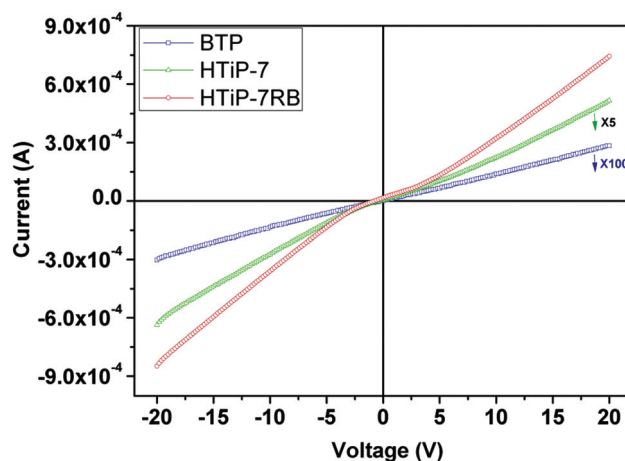

Fig. 12 UV-Vis reflectance spectra of BTP, HTiP-7, HTiP-7RB.

Fig. 14 I–V plot of BTP, HTiP-7, HTiP-7RB.
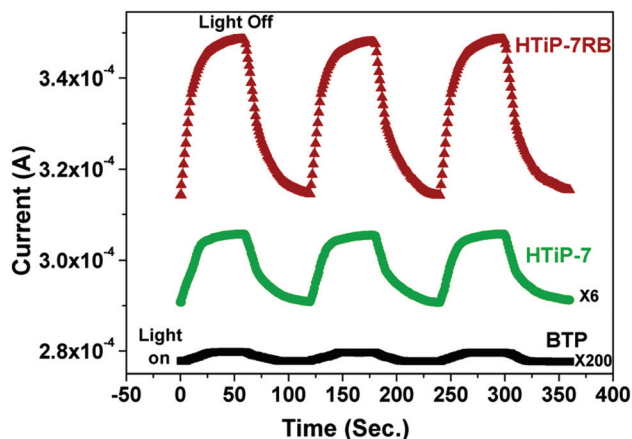
Fig. 15   Growth and decay current of BTP, HTiP-7, HTiP-7RB.

Scheme 1   Schematic representation of electron flow in the dye loaded HTiP-7 in the presence of light.

the current reaches 3.48×10^{-4} A for organic dye doped titanium phosphonate, 5.09×10^{-5} A for hybrid titanium phosphonate and 1.39×10^{-6} A for bulk titanium phosphate. Hence the photogenerated current ΔI (photocurrent minus dark current)[19] for photosensitizer doped titanium phosphonate is 0.35×10^{-4} A, while for hybrid titanium phosphonate it is 0.26×10^{-5} A and 0.1×10^{-6} A for bulk titanium phosphate. These results indicate that dye doped self assembled mesoporous titanium phosphonate nanoparticles (HTiP-7RB) generate 13.5 times more photocurrent than hybrid titanium phosphonate (HTiP-7) and 3500 times more photocurrent than bulk titanium phosphate (BTP). The interest in interfacial electron transfer pathways is increasing day by day due to the exciting solar cell application of the various TiO_2 based nanomaterials.[35] The mechanism of electron transfer involves the adsorption of various sensitizer molecules on the surface of semiconductor materials with a wide band gap.[36] The incorporation of a sensitizer molecule into the porous semiconductor materials helps visible light driven photoconductivity.[37] Now when we irradiate HTiP-7RB with light, the optical excitation of the RB injects an electron from its excited state to the conduction band of the porous hybrid titanium phosphonate.[38] This interfacial electron transfer process is much faster than the decay of the excited state of RB to its ground state.[39] The injected electron to the conduction band of titanium phosphonate is transported by diffusion to the oxidized dye and completes the total electrical circuit through the platinum electrode (Scheme 1).[40] But when we excite the hybrid titanium phosphonate and bulk titanium phosphate with white light, no such electron transfer process takes place without the transfer of an electron from the valence band to the conduction band of the materials. Due to the large band gap (3.2 eV) for bulk titanium phosphate, it produces minimum photocurrent (0.1×10^{-6} A) compared to hybrid titanium phosphonate nanoparticles. The band gap energy and photocurrent for hybrid titanium phosphonate is 2.98 eV and 0.26×10^{-5} A. Thus, excitation of electrons from the photosensitizer molecule and electron transfer inside the pores of semiconductor titanium
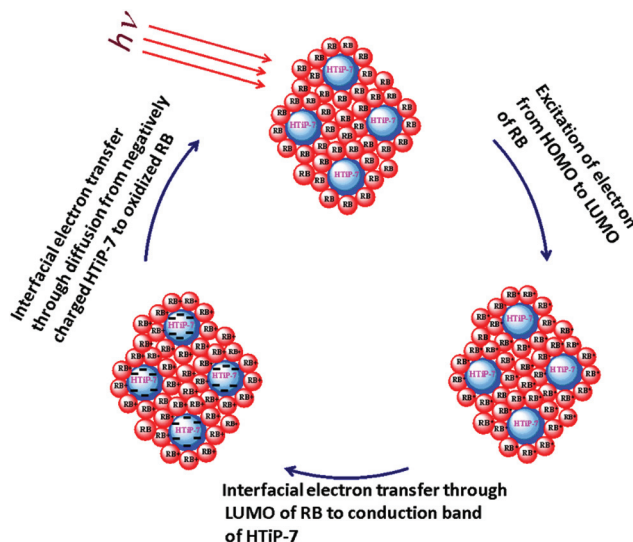
phosphonate enhance its visible light driven generation of photocurrent.

Conclusion

A new mesoporous hybrid titanium(IV) phosphonate nanomaterial has been synthesized by using benzene-1,3,5-triphosphonic acid as the organophosphorus source in the absence of any template molecule. The origin of the small angle XRD peak and mesoporosity in this material is due to the self-assembly of tiny nanocrystals of titanium phosphonate and the surface interactions of the aggregated nanoparticles. The material has been assigned with a new triclinic crystal phase. It showed high BET surface area (255 $m^2 g^{-1}$) together with a pore volume of 0.46 cc g^{-1}. Porosity of the material has been utilized for the impregnation of the photosensitizer molecule (dye) inside the pores. The photocurrent generated by sensitizer entrapped titanium phosphonate material is quite higher than other titanium oxide based nanomaterials. Thus, we can design different hybrid titanium phosphonate materials bearing organic functionalities to enhance the efficiency of the photon-to-electron energy transfer process. Alongside, the hybrid titanium phosphonate material with nanoscale porosity may have potential biological applications in drug delivery and in lithium ion batteries.

Acknowledgements

Notes and references

1 (*a*) D. A. Loyt and K. J. Shea, *Chem. Rev.*, 1995, **95**, 1431–1442; (*b*) A. Stein, B. J. Melde and R. C. Schroden, *Adv. Mater.*, 2000, **12**, 1403–1419; (*c*) F. Hoffmann, M. Cornelius, J. Morell and M. Froba, *Angew. Chem., Int. Ed.*, 2006, **45**, 3216–3251; (*d*) Y. Maegawa, N. Mizoshita, T. Tani and S. Inagaki, *J. Mater. Chem.*, 2010, **20**, 4399–4403.

2 T. Y. Ma, X. Z. Lin and Z. Y. Yuan, *Chem.–Eur. J.*, 2010, **16**, 8487–8494.

3 T. Y. Ma, X. J. Zhang and Z. Y. Yuan, *Microporous Mesoporous Mater.*, 2009, **123**, 234–242.

4 (*a*) A. Clearfield, *Dalton Trans.*, 2008, 6089–6102; (*b*) A. Dutta, A. K. Patra and A. Bhaumik, *Microporous Mesoporous Mater.*, 2012, **155**, 208–214; (*c*) M. Richter, A. Karschin, B. Spingler, P. C. Kunz, W. Meyer-Zaika and W. Klaeui, *Dalton Trans.*, 2012, **41**, 3407–3413.

5 A. Aklil, M. Mouflihb and S. Sebti, *J. Hazard. Mater.*, 2004, **112**, 183–190.

6 (*a*) K. J. Gagnon, A. V. Prosvirin, K. R. Dunbar, S. J. Teat and A. Clearfield, *Dalton Trans.*, 2012, **41**, 3995–4006; (*b*) F. Tong, Z. G. Sun, K. Chen, Y. Y. Zhu, W. N. Wang, C. Q. Jiao, C. L. Wang and C. Li, *Dalton Trans.*, 2011, **40**, 5059–5065; (*c*) T. Y. Ma and Z. Y. Yuan, *Dalton Trans.*, 2010, **39**, 9570–9578.

7 A. Clearfield, *Chem. Mater.*, 1998, **10**, 2801–2810.

8 (*a*) G. Cao, H. G. Hong and T. E. Mallouk, *Acc. Chem. Res.*, 1992, **25**, 420–427; (*b*) P. Barber, H. Houghton, S. Balasubramanian, Y. K. Anguchamy, H. J. Ploehn and H. C. z. Loye, *Chem. Mater.*, 2009, **21**, 1303–1310.

9 (*a*) G. Alherti, U. Costantino, F. Marmottini, R. Vivani and P. Zappelli, *Angew. Chem., Int. Ed. Engl.*, 1993, **32**, 1357–1359; (*b*) M. V. Vasylyev, E. J. Wachtel, R. P. Biro and R. Neumann, *Chem.–Eur. J.*, 2006, **12**, 3507–3514.

10 (*a*) M. Vasylyev and R. Neumann, *Chem. Mater.*, 2006, **18**, 2781–2783; (*b*) G. Guerrero, P. H. Mutin and A. Vioux, *Chem. Mater.*, 2000, **12**, 1268–1272.

11 (*a*) Y. Cao, L. Jing, X. Shi, Y. Luan, J. R. Durrant, J. Tang and H. Fu, *Phys. Chem. Chem. Phys.*, 2012, **14**, 8530–8536; (*b*) L. Korosi, S. Papp, I. Bertoti and I. Dekany, *Chem. Mater.*, 2007, **19**, 4811–4819.

12 C. D. Valentin and D. Costa, *J. Phys. Chem. C*, 2012, **116**, 2819–2828.

13 A. Milo and R. Neumann, *Adv. Synth. Catal.*, 2010, **352**, 2159–2165.

14 (*a*) X. J. Zhang, T. Y. Ma and Z. Y. Yuan, *J. Mater. Chem.*, 2008, **18**, 2003–2010; (*b*) A. Bhaumik and S. Inagaki, *J. Am. Chem. Soc.*, 2001, **123**, 691–696.

15 (*a*) T. Y. Ma, L. Liu, Q. F. Deng, X. Z. Lin and Z. Y. Yuan, *Chem. Commun.*, 2011, **47**, 6015–6017; (*b*) T. Y. Ma, X. Z. Lin and Z. Y. Yuan, *J. Mater. Chem.*, 2010, **20**, 7406–7415.

16 Y. Sagatelian, D. Sharabi and Y. Paz, *J. Photochem. Photobiol., A*, 2005, **174**, 253–260.

17 A. Dutta, A. K. Patra, S. Dutta, B. Saha and A. Bhaumik, *J. Mater. Chem.*, 2012, **22**, 14094.

18 G. Facchin, F. Minto, M. Gleria, R. Bertani and P. Bortolus, *J. Inorg. Organomet. Polym.*, 1991, **1**, 389–395.

19 (*a*) A. K. Patra, S. K. Das and A. Bhaumik, *J. Mater. Chem.*, 2011, **21**, 3925–3930; (*b*) N. Pal, M. Paul, A. Bera, D. Basak and A. Bhaumik, *Anal. Chim. Acta*, 2010, **674**, 96–101.

20 (*a*) S. Kwon, J. H. Park, H. Chung, I. C. Kwon and S. Y. Jeong, *Langmuir*, 2003, **19**, 10188–10193; (*b*) J. H. Parka, S. Kwona, M. Lee, H. Chunga, J. H. Kimc, Y. S. Kimc, R. W. Parkc, I. S. Kimc, S. B. Seod, I. C. Kwon and S. Y. Jeong, *Biomaterials*, 2006, **27**, 119–126.

21 D. Kong, J. Zon, J. McBee and A. Clearfield, *Inorg. Chem.*, 2006, **45**, 977–986.

22 Y. Zhou and M. Antonietti, *J. Am. Chem. Soc.*, 2003, **125**, 14960–14961.

23 S. Han, S. H. Choi, S. S. Kim, M. Cho, B. Jang, D. Y. Kim, J. Yoon and T. Hyeon, *Small*, 2005, **1**, 812–816.

24 T. Y. Ma, H. Li, A. N. Tang and Z. Y. Yuan, *Small*, 2011, **7**, 1827–1837.

25 K. Sarkar, T. Yokoi, T. Tatsumi and A. Bhaumik, *Microporous Mesoporous Mater.*, 2008, **110**, 405–412.

26 R. D. Cakan, Y. S. Hu, M. Antonietti, J. Maier and M. M. Titirici, *Chem. Mater.*, 2008, **20**, 1227–1229.

27 (*a*) D. Chandra, N. Mukherjee, A. Mondal and A. Bhaumik, *J. Phys. Chem. C*, 2008, **112**, 8668–8674; (*b*) R. Ryoo, I. S. Park, S. Jun, C. W. Lee, M. Kruk and M. Jaroniec, *J. Am. Chem. Soc.*, 2001, **123**, 1650–1657.

28 M. Pramanik, M. Nandi, H. Uyama and A. Bhaumik, *Catal. Sci. Technol.*, 2012, **2**, 613–620.

29 (*a*) M. Kruk and M. Jaroniec, *Chem. Mater.*, 2001, **13**, 3169–3183; (*b*) S. K. Das, M. K. Bhunia and A. Bhaumik, *Dalton Trans.*, 2010, **39**, 4382–4390.

30 P. I. Ravikovitch and A. V. Neimark, *J. Phys. Chem. B*, 2001, **105**, 6817–6823.

31 (*a*) Y. Segawa, A. Fukazawa, S. Matsuura, H. Omachi, S. Yamaguchi, S. Irle and K. Itami, *Org. Biomol. Chem.*, 2012, **10**, 5979–5984; (*b*) Y. R. Morales, *J. Phys. Chem. A*, 2002, **106**, 11283–11308.

32 (*a*) R. Memming and H. Tributsch, *J. Phys. Chem.*, 1971, **75**, 562–570; (*b*) H. Ross, J. Bendig and S. Hecht, *Sol. Energy Mater. Sol. Cells*, 1994, **33**, 475–481.

33 C. G. Shuttle, A. Maurano, R. Hamilton, B. O'Regan, J. C. de Mello and J. R. Durrant, *Appl. Phys. Lett.*, 2008, **93**, 183501.

34 D. Chandra, S. Mridha, D. Basak and A. Bhaumik, *Chem. Commun.*, 2009, 2384–2386.

35 B. O'Regan and M. Gratzel, *Nature*, 1991, **353**, 737–740.

36 N. Vlachopoulos, P. Liska, J. Augustynski and M. Gratzel, *J. Am. Chem. Soc.*, 1988, **110**, 1216–1220.

37 N. C. Greenham, X. Peng and A. P. Alivisatos, *Phys. Rev. B: Condens. Matter*, 1996, **54**, 17628–17637.

38 Y. Tachibana, S. A. Haque, I. P. Mercer, J. R. Durrant and D. R. Klug, *J. Phys. Chem. B*, 2000, **104**, 1198–1205.

39 J. B. Asbury, R. J. Ellingson, H. N. Ghosh, S. Ferrere, A. J. Nozik and T. Lian, *J. Phys. Chem. B*, 1999, **103**, 3110–3119.

40 S. Kambe, S. Nakade, T. Kitamura, Y. Wada and S. Yanagida, *J. Phys. Chem. B*, 2002, **106**, 2967–2972.